

Supporting Information

Ionothermal synthesis of three-dimensional hierarchical Ni₃Se₂ mesoporous nanosheet network with enhanced performance for asymmetric supercapacitors

Yanxia Liu^a, Qiuchen Xu^a, Ran Wang^a, Yiteng Zheng^{*b}, Lianjie Zhu^c, Zhen Wang^d, Wenjun Zheng^{*a, e}

- a. Department of Chemistry, Key Laboratory of Advanced Energy Materials Chemistry (MOE), TKL of Metal and Molecule-based Material Chemistry, College of Chemistry, Nankai University, Tianjin, 300071, P. R. China.
- b. Department of Chemical Engineering and Materials Science, Stevens Institute of Technology, Hoboken, New Jersey 07030, United States.
- c. School of Chemistry & Chemical Engineering, Tianjin Key Laboratory of Organic Solar Cells and Photochemical Conversion, Tianjin University of Technology, Tianjin 300384, P. R. China.
- d. Key Laboratory of Materials Processing and Mold (Zhengzhou University), Ministry of Education, Zhengzhou University, Zhengzhou 450002, P. R. China.
- e. Collaborative Innovation Center of Chemical Science and Engineering, Nankai University, Tianjin, 300071, P. R. China.

* Corresponding author E-mail: zhwj@nankai.edu.cn (W. Zheng), yzheng3@stevens.edu (Y. Zheng)

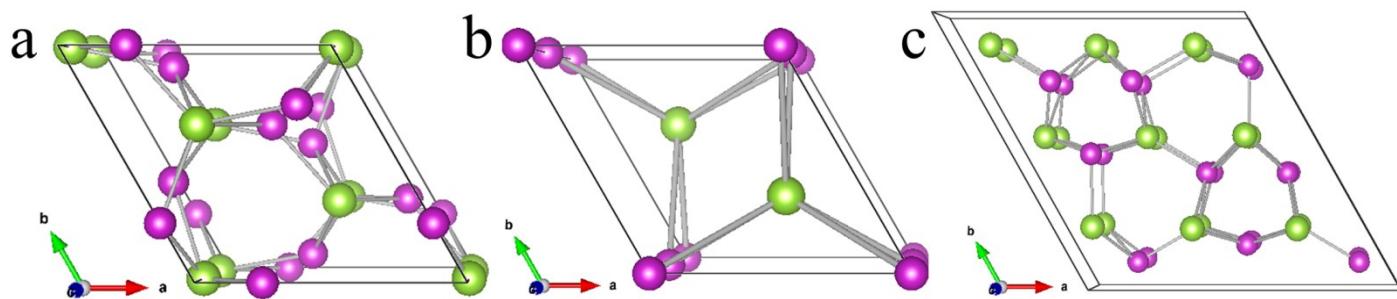


Figure S1. Schematic illustrations of crystal structures of (a) Ni_3Se_2 (JCPDS No. 19-0841), (b) NiSe (JCPDS No. 89-7160) and (c) NiSe (JCPDS No. 89-2058). Green balls are Se atoms and purple balls are Ni atoms.

As the crystal structure of the hexagonal Ni_3Se_2 shows, Ni atoms are coordinated to four Se atoms and four Ni atoms. In the crystal structure of the hexagonal NiSe (JCPDS No. 89-7160), Ni atoms coordinate with six Se atoms to form an octahedron, and Se atoms coordinate with six Ni atoms to form a pentahedron. As regards the crystal structure of the hexagonal NiSe (JCPDS No. 89-2058), Ni atoms are 5-fold coordinated to Se atoms and Se atoms are 5-fold coordinated to Ni atoms.

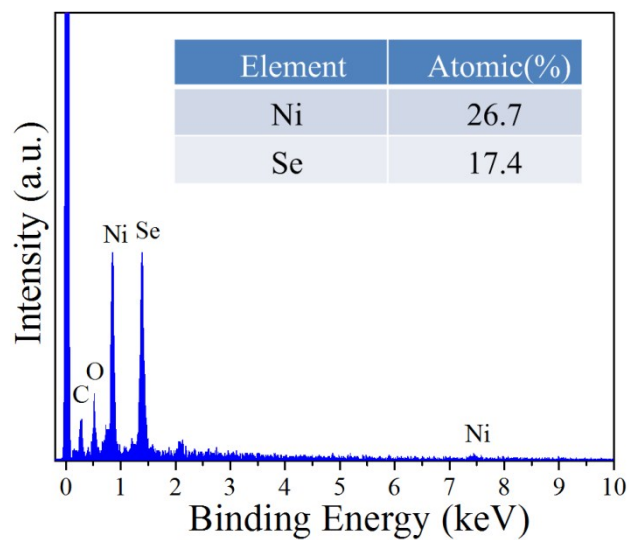


Figure S2. EDX spectrum of the Ni_3Se_2 3D HMNN. Note: C and O signals arise from conductive tape substrate and adsorbed water, respectively.

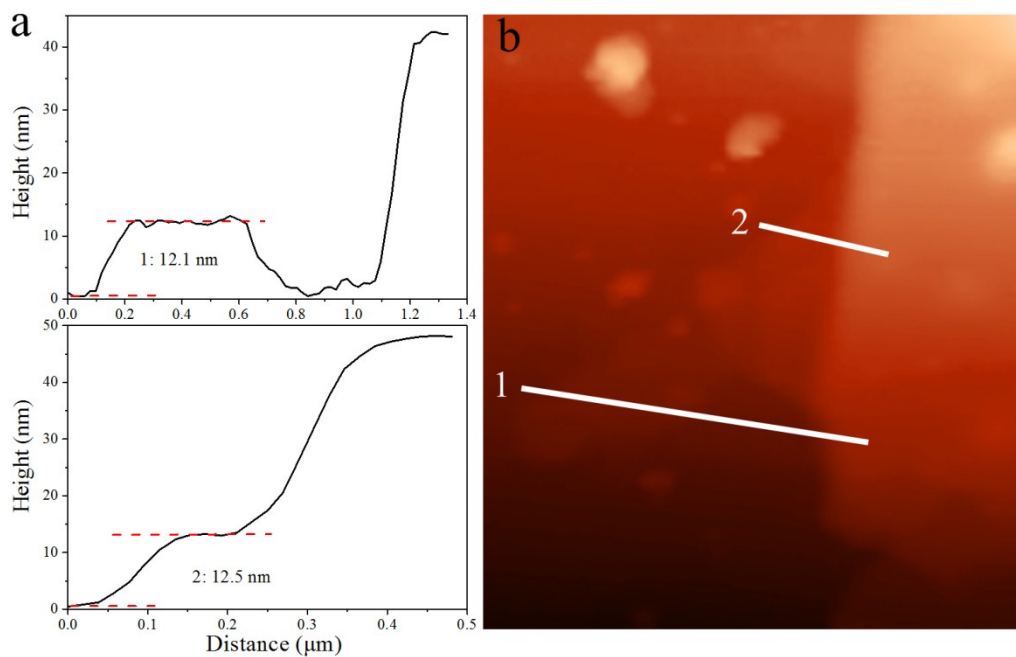


Figure S3. (a) Height profiles derived from the AFM image. (b) AFM image of the Ni₃Se₂ nanosheets.

Notably, the numbers 1 and 2 in (a) correspond to 1 and 2 in (b), respectively.

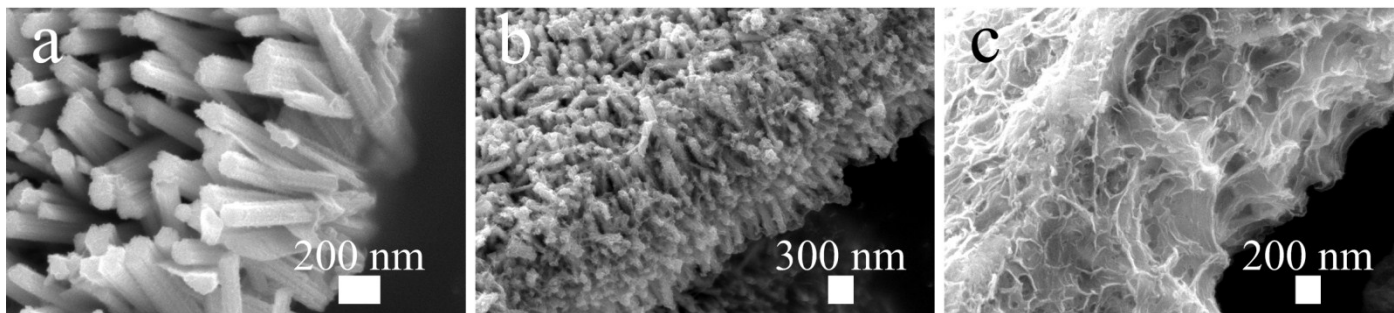


Figure S4. Side-view FESEM images of the as-prepared products in the presence of different amount of [BMIm]Cl: (a) 0, (b) 20 and (c) 40 mmol.

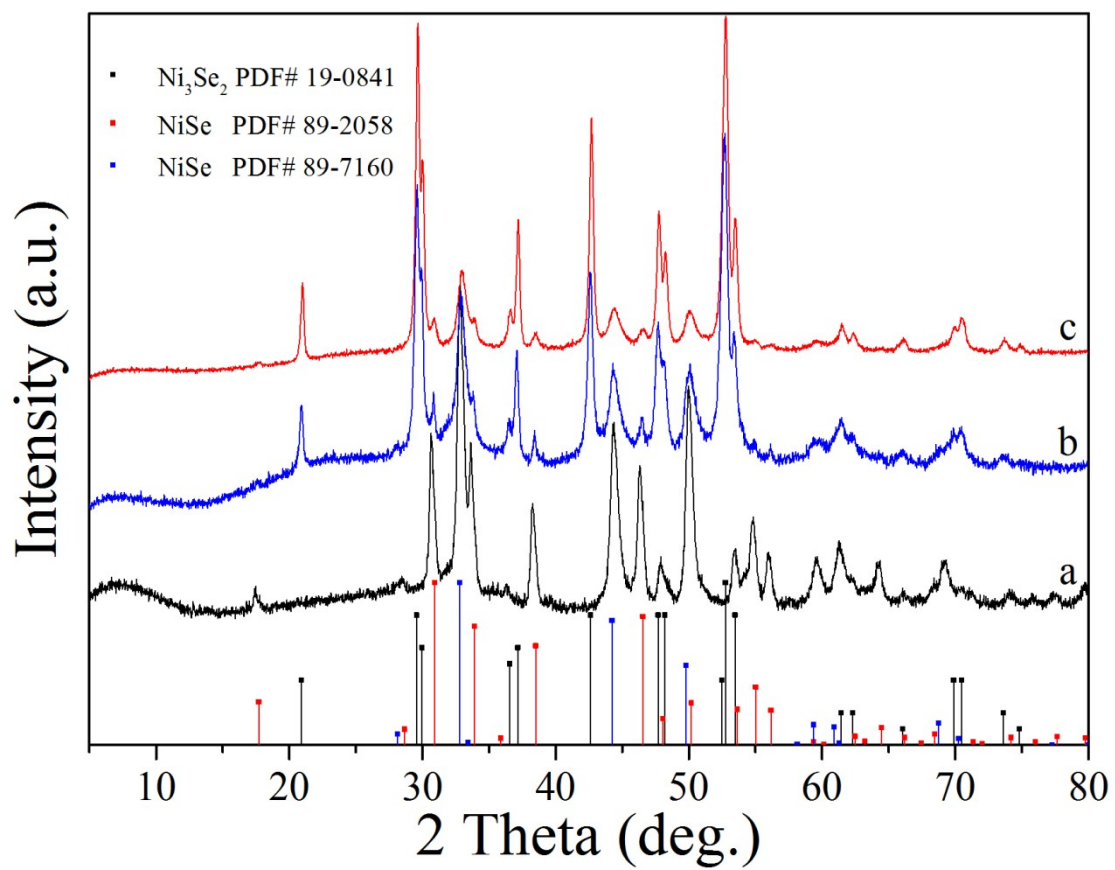


Figure S5. XRD patterns of the products prepared using different amount of [BMIm]Cl: (a) 0, (b) 20 and (c) 40 mmol.

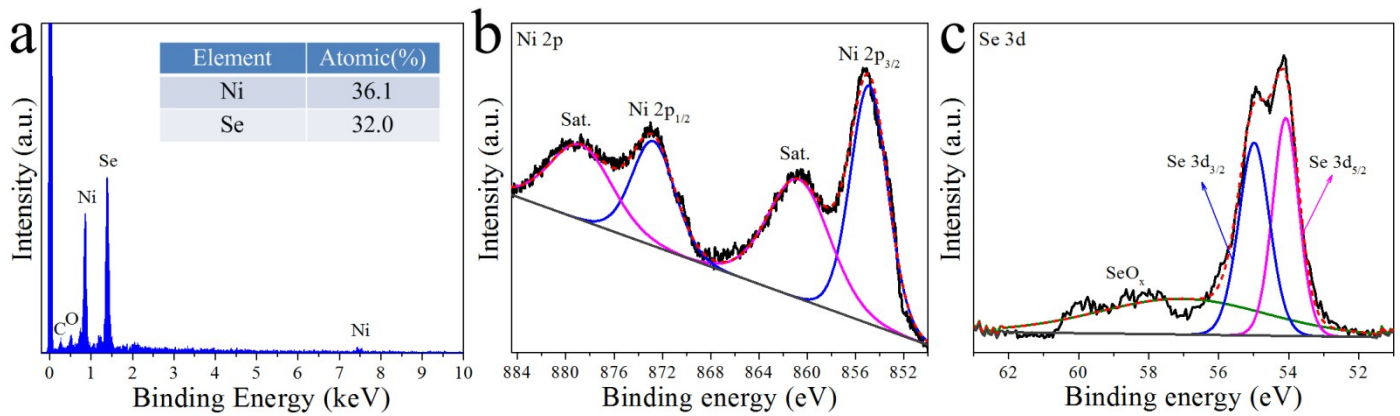


Figure S6. Characterizations of the 1D NiSe NRs: (a) EDX spectrum. Note: C and O signals arise from conductive tape substrate and adsorbed water, respectively. (b, c) XPS spectra of Ni 2p and Se 3d.

XPS spectra of the 1D NiSe NRs was recorded to investigate its elemental chemical states, as shown in **Figure S6b** and **c**. The Ni 2p spectrum can be best fitted with two spin-orbit doublets and two shake-up satellites (marked “Sat.”). The peaks at 854.9 eV in Ni 2p_{3/2} and 872.7 eV in Ni 2p_{1/2} correspond to the spin-orbit characteristic of Ni²⁺.^{S1} Furthermore, the peaks at 860.7 and 878.7 eV are the corresponding shake-up satellites. As regards the Se 3d spectrum, the broad peak at about 57.0 eV suggests surface oxidation of the Se⁴⁺ species. Moreover, the peaks at 54.1 and 55.0 eV are representative of the Se 3d_{5/2} and Se 3d_{3/2} of Se²⁻.^{S2} All these results prove that 1D NiSe NRs have been successfully synthesized.

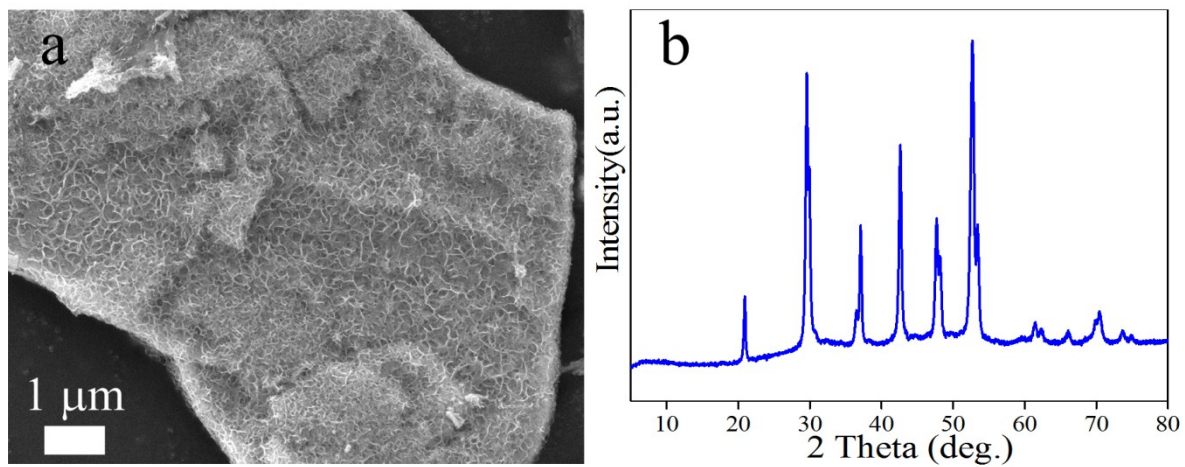


Figure S7. (a) FESEM image and (b) XRD pattern of the product prepared by using equimolar of [BMIm]Ac instead of [BMIm]Cl.

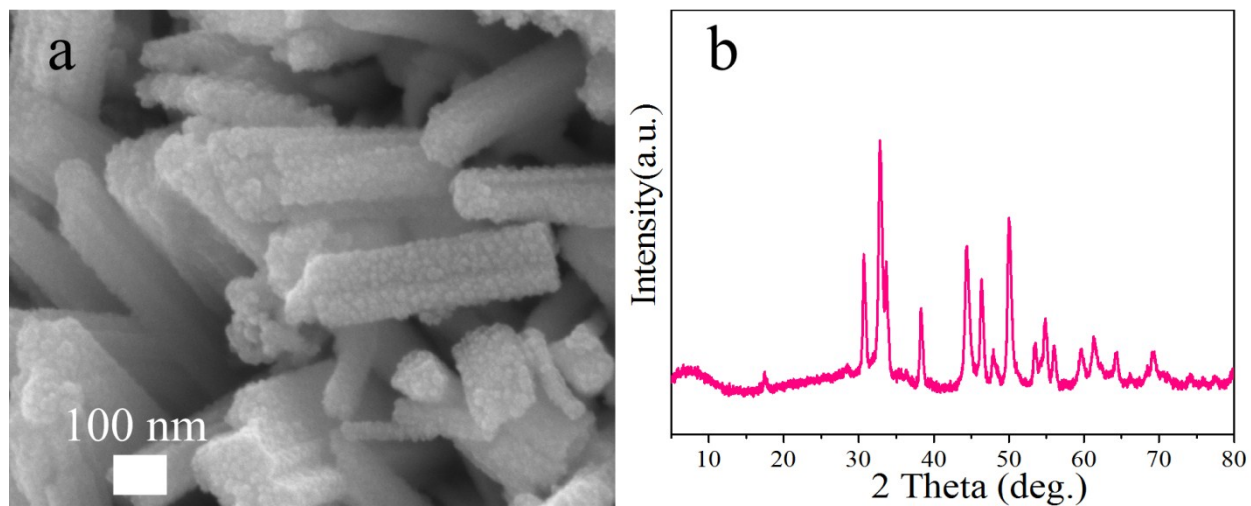


Figure S8. (a) FESEM image and (b) XRD pattern of the product prepared by using equimolar of NaCl instead of [BMIm]Cl.

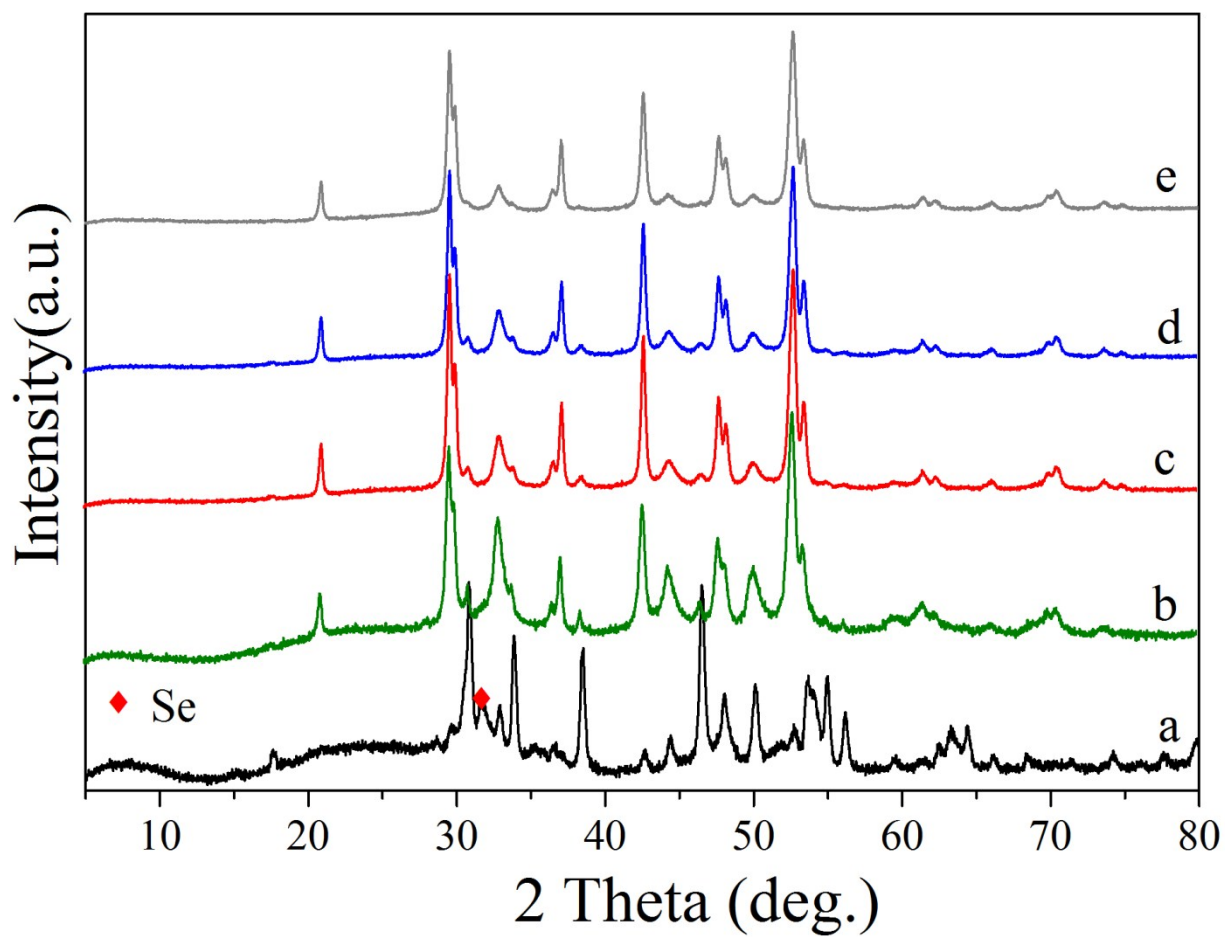


Figure S9. XRD patterns of the as-prepared products in the presence of 60 mmol of [BMIm]Cl for different reaction time intervals: (a) 4, (b) 8, (c) 12, (d) 16 and (e) 20 h.

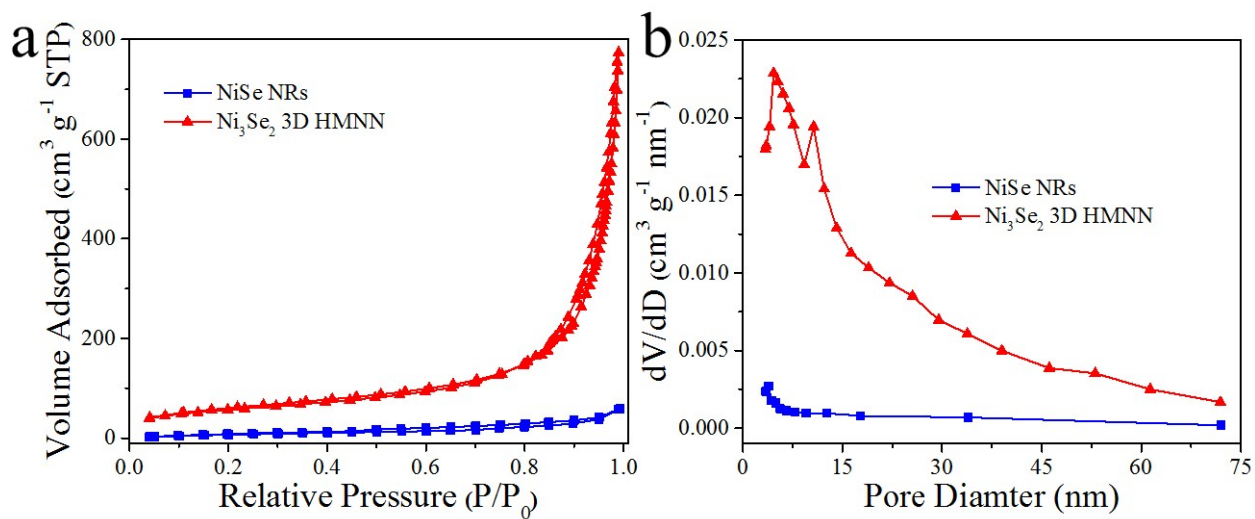


Figure S10. (a) N_2 adsorption-desorption isotherms and (b) BJH pore size distribution plots for the Ni_3Se_2 3D HMNN and 1D NiSe NRs.

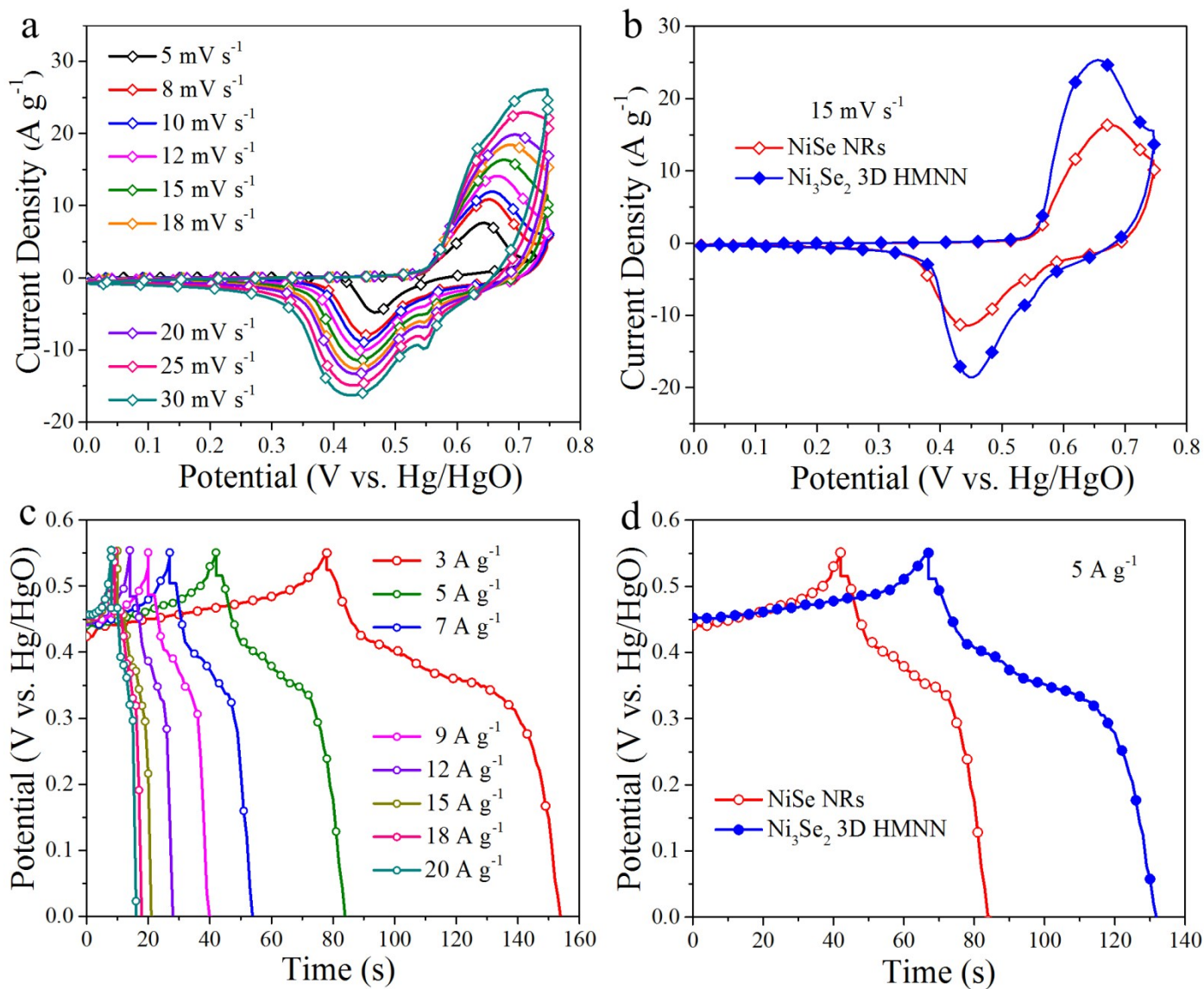


Figure S11. (a) CV curves of the 1D NiSe NRs at various scan rates. (b) CV curves of the Ni₃Se₂ 3D HMNN and 1D NiSe NRs at scan rate of 15 mV s⁻¹. (c) GCD curves of the 1D NiSe NRs at different current densities. (d) GCD curves of the Ni₃Se₂ 3D HMNN and 1D NiSe NRs at current density of 5 A g⁻¹.

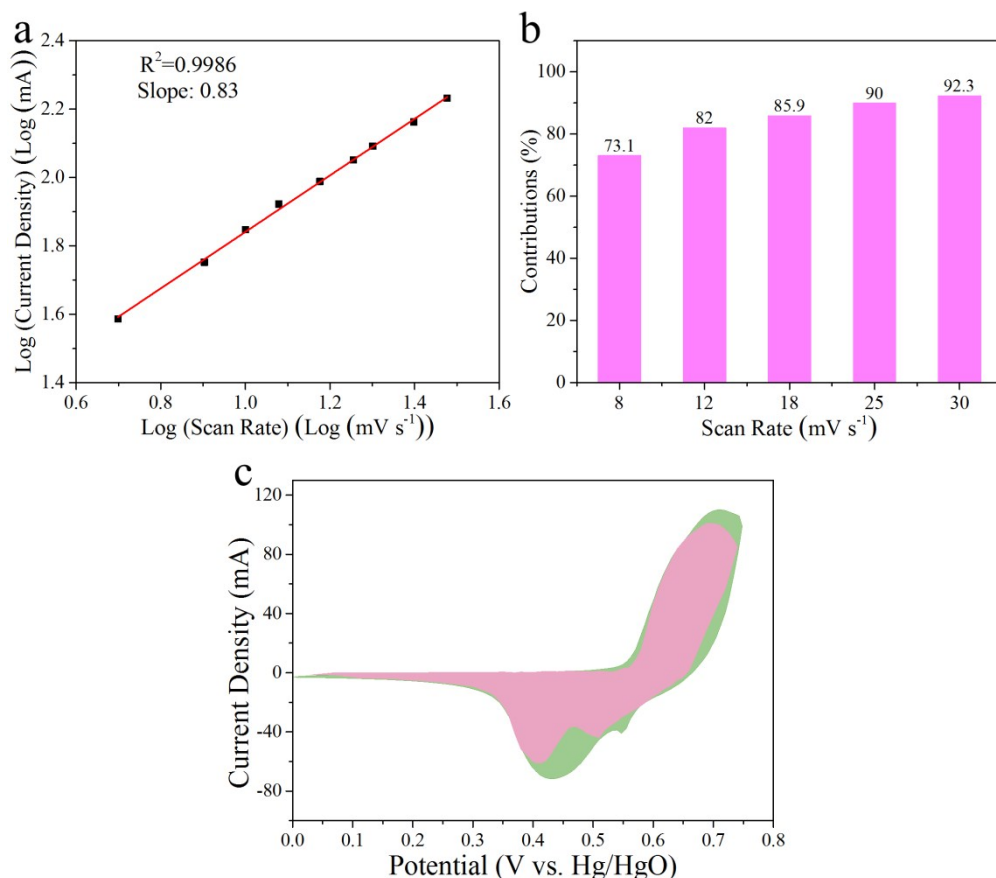


Figure S12. (a) Determination of the b -value using the relationship between the peak current and the scan rate. (b) Bar chart showing the percentage contribution from capacitive effect at different scan rates for the Ni_3Se_2 3D HMNN electrode. (c) The capacitive effect contribution of the Ni_3Se_2 3D HMNN electrode at a scan rate of 12 mV s^{-1} .

According to the previous reports, the peak current (i) and the scan rate (ν) comply with the following equations:^{S3}

$$i = a\nu^b \tag{1}$$

$$\log(i) = b\log(\nu) + \log(a) \tag{2}$$

The value of b is 1 (namely, $i = a\nu$), involving to nondiffusion-controlled surface redox reaction (capacitive effect), whereas b equals to $1/2$ (that is, $i = a\nu^{1/2}$), involving to diffusion-controlled redox intercalation process (battery-type behavior). **Figure S13a** shows the fitted line of the Ni_3Se_2 3D HMNN electrode based on the anodic peaks with the b -value of 0.83, which reveals that the current arises from capacitive effect mixed with contributions from diffusion-controlled battery-type behavior. It is reported that thin nanosheets

often exhibit both capacitive and battery-type behavior because of reversible intercalation of ions.^{S4} The ratio of the contribution of the surface capacitive effect (surface double-layer capacitance and pseudocapacitance) to that of diffusion-controlled process (battery-type behavior) for the Ni₃Se₂ 3D HMNN can be analyzed and calculated on the basis of the following equations:^{S3,S4}

$$i = k_1v + k_2v^{1/2}$$

(3)

$$i/v^{1/2} = k_1v^{1/2} + k_2$$

(4)

The current response at a fixed potential is described as a sum of two mechanisms (surface capacitive effects k_1v and diffusion-controlled intercalation processes $k_2v^{1/2}$), k_1 and k_2 are constants and can be determined by plotting $v^{1/2}$ versus $i/v^{1/2}$, thus ratio of surface capacitive charge storages to the total charge storages for the Ni₃Se₂ 3D HMNN electrode can be determined. As displayed in **Figure S13b**, with increasing the scan rate, the capacitive contributions of the Ni₃Se₂ 3D HMNN electrode increases while the intercalation contribution decreases because of inadequate insertion of OH⁻ from alkaline electrolyte into the Ni₃Se₂ 3D HMNN. Therefore, the surface capacitive mechanism dominate the excellent electrochemical performance of the Ni₃Se₂ 3D HMNN. **Figure S13c** shows that about 82% of the total capacitance comes from the surface capacitive effect at a scan rate of 12 mV s⁻¹.

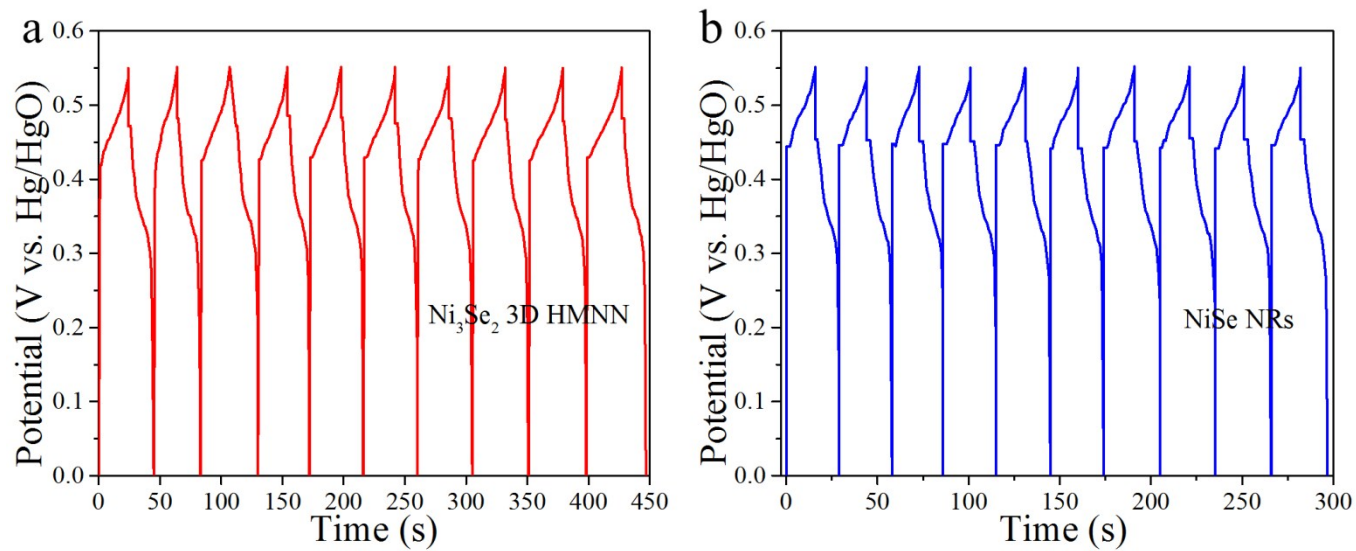


Figure S13. The first 10 cycles of galvanostatic charge-discharge voltage profiles at a large current density of 10 A g⁻¹: (a) the Ni₃Se₂ 3D HMNN, (b) the 1D NiSe NRs.

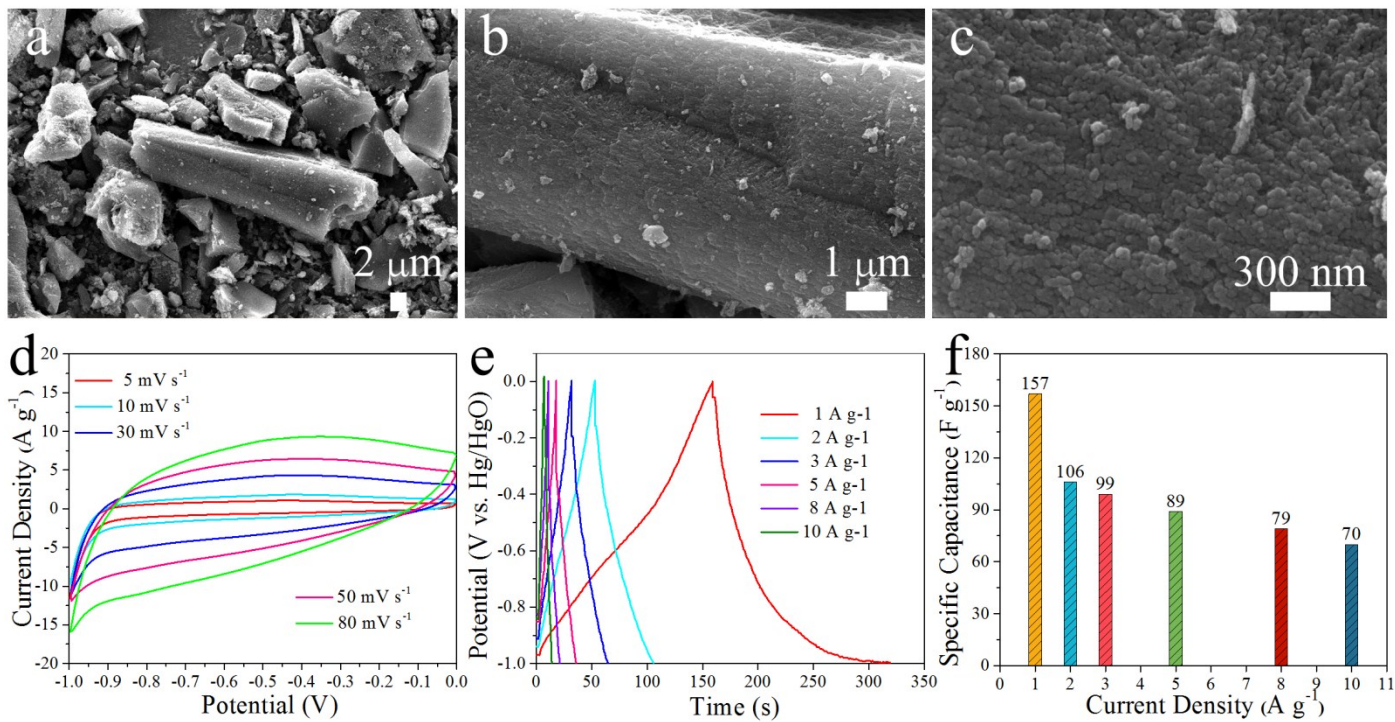


Figure S14. (a-c) FESEM images of AC. (d) CV curves of AC at various scan rates. (e) GCD curves of AC at different current densities. (f) Rate performance of AC from 1 to $10\ \text{A g}^{-1}$.

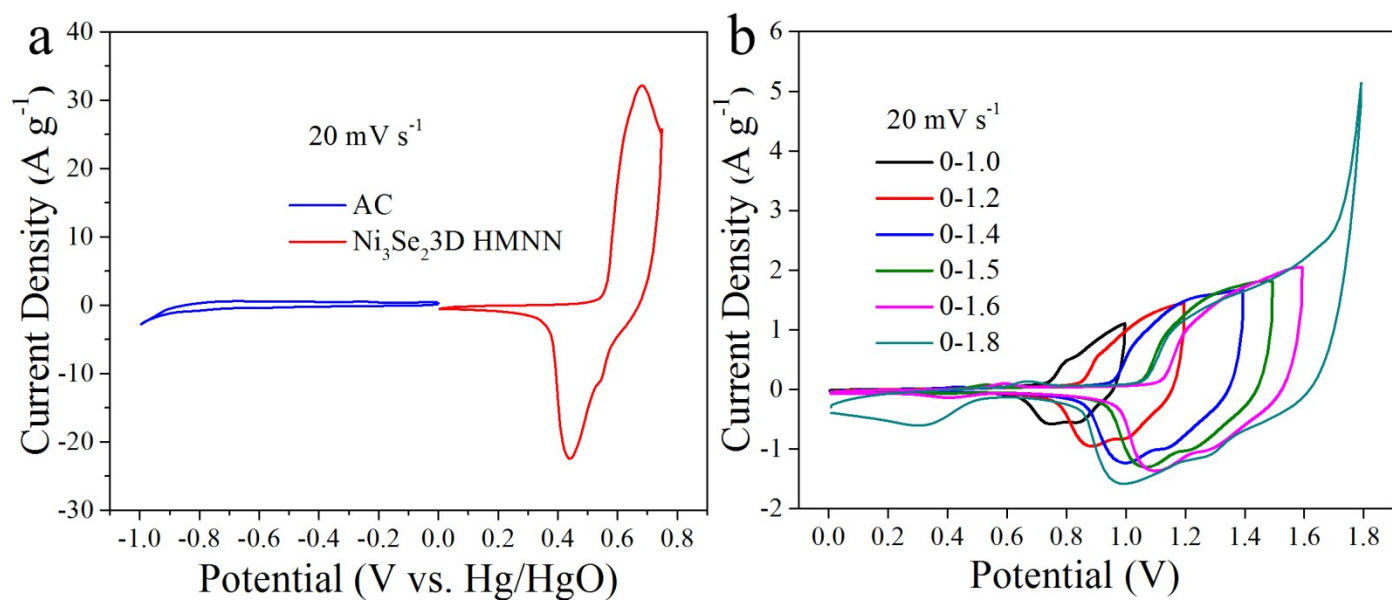


Figure S15. (a) Comparative CV curves of AC and the Ni₃Se₂ 3D HMNN at a scan rate of 20 mV s⁻¹ in a three-electrode system. (b) CV curves of the as-assembled Ni₃Se₂ 3D HMNN//AC ASC device measured at different voltage windows at a scan rate of 20 mV s⁻¹.

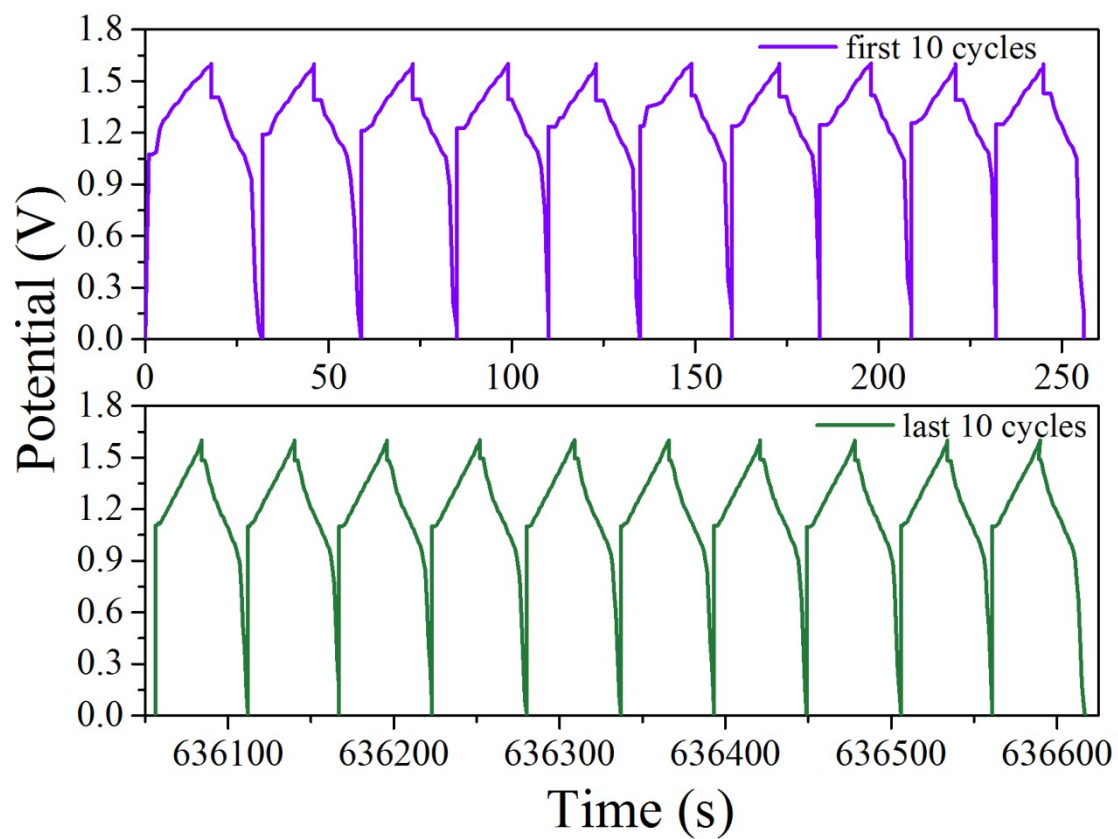


Figure S16. First and last 10 GCD curves of the Ni_3Se_2 3D HMNN//AC ASC device for 10000 cycles at 2 A g^{-1} .

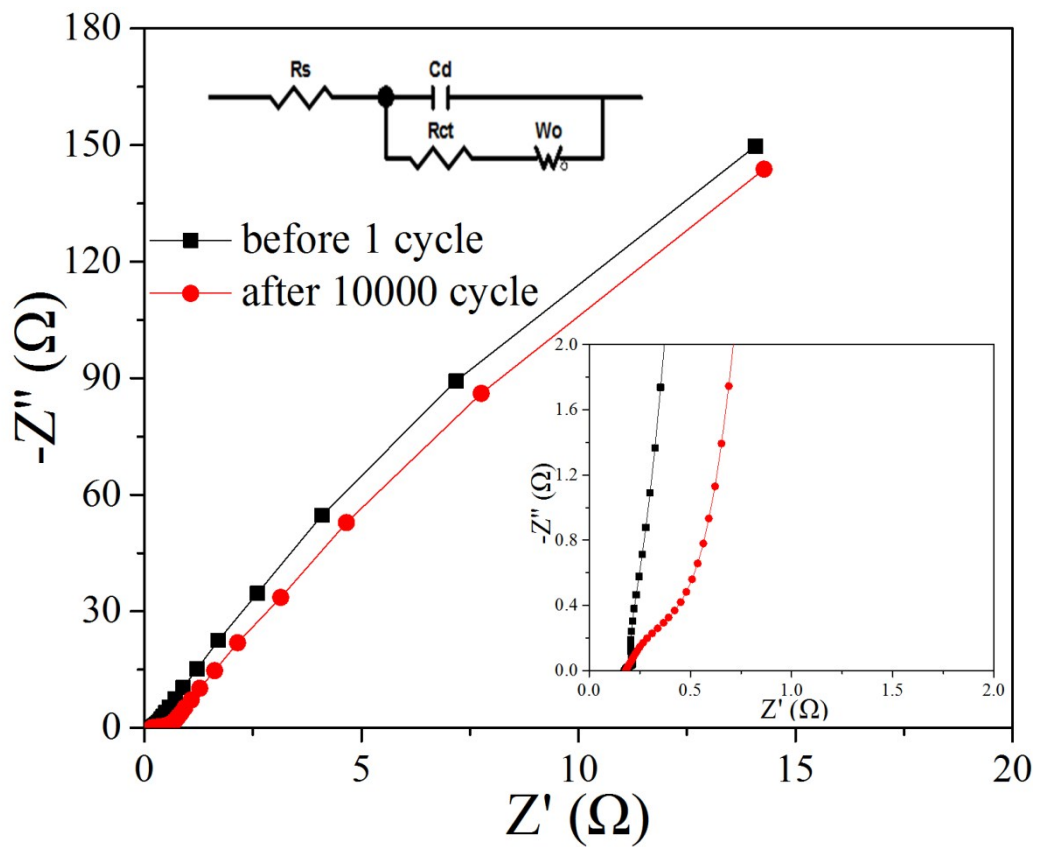


Figure S17. Impedance Nyquist plots of the Ni₃Se₂ 3D HMNN//AC ASC device before the 1th cycle and after the 10000th cycle (The top left and low right corner insets are the corresponding equivalent circuit and amplification pattern, respectively).

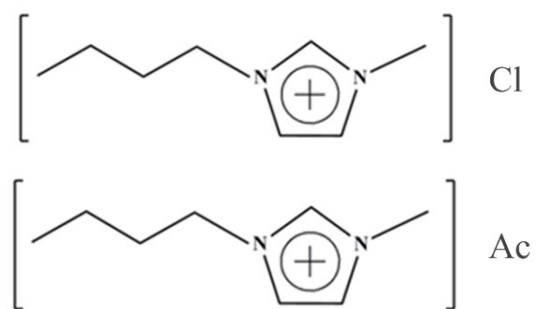


Figure S18. Structures of [BMIm]Cl (1-butyl-3-methylimidazolium chloride) and [BMIm]Ac (1-butyl-3-methylimidazolium acetate).

Table S1. Comparison of the morphology and synthesis method of Ni₃Se₂ HMNN with other previously reported Ni₃Se₂-based materials.

Morphology	Synthesis method	Ref.
Ni ₃ Se ₂ nanowires	solvothermal	S5
Ni ₃ Se ₂ nanowire arrays	solvothermal	S6
cauliflower-like Ni ₃ Se ₂	electrochemical deposition	S7
Ni ₃ Se ₂ film	electrochemical deposition	S8
Ni ₃ Se ₂ nanoforest	solution chemical route	S9
Ni ₃ Se ₂ nanorod array	solvothermal	S10
Ni ₃ Se ₂ microspheres	hydrothermal	S11
Ni ₃ Se ₂ nanosheet arrays	hydrothermal	S12
Ni ₃ Se ₂ nanoparticles	γ -ray irradiation	S13
rod-like Ni ₃ Se ₂	solvothermal	S14
Ni ₃ Se ₂ bulks	solvothermal	S15
Ni ₃ Se ₂ mesoporous nanosheet network	ionothermal	This work

Table S2. Surface area, BJH pore size and total pore volume of the Ni₃Se₂ 3D HMNN and 1D NiSe NRs.

Samples	Surface area (m ² g ⁻¹)	Pore size (nm)	Pore volume (cm ³ g ⁻¹)
Ni ₃ Se ₂ 3D HMNN	201.2	4.6, 10.6	0.658
1D NiSe NRs	12.3	3.8	0.048

Table S3. Comparison of electrochemical performance of the Ni₃Se₂ 3D HMNN with other previously reported Ni-based active materials in a three-electrode system.

Electrode materials	Current collector	Specific capacitance	Cyclic stability	Electrolyte	Ref.
Ni ₃ Se ₂ nanowires	Ni foam	635 mA h cm ⁻² at 3 mA cm ⁻²	-	3 M KOH	S5
Ni ₃ Se ₂ nanowire arrays	Ni foam	635 mA h cm ⁻² at 3 mA cm ⁻²	-	3 M KOH	S6
cauliflower-like Ni ₃ Se ₂	conductive fabric	119.6 mAh g ⁻¹ at 2 A g ⁻¹	-	1 M KOH	S7
V ₂ O ₅ @Ni ₃ S ₂	Ni foam	854 F g ⁻¹ at 1 A g ⁻¹	60% for 1000 cycles at 1 A g ⁻¹	1 M KOH	S16
CoNiSe ₂ nanorods	Ni foam	0.5 mAh cm ⁻²	83.7% for 5000 cycles at 20 mA cm ⁻²	1 M KOH	S17
NiCo ₂ S ₄ hollow nanoneedle	Carbon paper	1154 F g ⁻¹ at 1 A g ⁻¹	76.7% for 8000 cycles at 10 A g ⁻¹	2 M KOH	S18
NiSe@MoSe ₂ nanosheets array	Carbon cloth	769.2 F g ⁻¹ at 1 A g ⁻¹	93.7% for 1000 cycles at 5 A g ⁻¹	2 M KOH	S19
PPy@3D Ni ^{a)}	Ti foil	726 F g ⁻¹ at 1 A g ⁻¹	95.8% for 1000 cycles at 100 mV s ⁻¹	1 M Na ₂ SO ₄	S20
NiCo ₂ S ₄ flaky structure	Ni foam	1366 F g ⁻¹ at 1 A g ⁻¹	89.8% for 2000 cycles at 10 A g ⁻¹	2 M KOH	S21
Ni-Tp/PANI ^{b)}	Ni foam	938.85 F g ⁻¹ at 1.8 A g ⁻¹	85.4% for 3000 cycles at 4.545 A g ⁻¹	3 M KOH	S22
Ni ₃ S ₂ nanowires	Ni foam	760 F g ⁻¹ at 0.5 A g ⁻¹	60% for 1000 cycles at 10 A g ⁻¹	2 M KOH	S23
Ni₃Se₂ 3D HMNN	Ni foam	801 F g⁻¹ at 3 A g⁻¹	80.2% for 10000 cycles at 10 A g⁻¹	3 M KOH	This work

^{a)}Polypyrrole (PPy) shell@3D-Ni-core; ^{b)} Nickel terephthalate/polyaniline

Table S4. The R_s , R_{ct} and Z_w values of the Ni_3Se_2 3D HMNN//AC ASC device before the 1st cycle and after the 10000th cycle.

Samples	R_s (Ω)	R_{ct} (Ω)	Z_w (Ω)
before the 1st cycle	0.181	0.051	0.018
after the 10000th cycle	0.195	0.552	0.005

References:

- S1 H. Chen, S. Chen, M. Fan, C. Li, D. Chen, G. Tian and K. Shu, *J. Mater. Chem. A*, 2015, 3, 23653.
- S2 X. Han, X. Tong, G. Wu, N. Yang and X.-Y. Guo, *Carbon*, 2018, 129, 245.
- S3 K. Zou, P. Cai, C. Liu, J. Li, X. Gao, L. Xu, G. Zou, H. Hou, Z. Liu and X. Ji, *J. Mater. Chem. A*, 2019, 7, 13540.
- S4 R. Wang, C. Xu and J.-M. Lee, *Nano Energy*, 2016, 19, 210.
- S5 X. Shi, J. Key, S. Ji, V. Linkov, F. Liu, H. Wang, H. Gai and R. Wang, *Small*, 2018, 1802861.
- S6 X. Shi, H. Wang, P. Kannan, J. Ding, S. Ji, F. Liu, H. Gai and R. Wang, *J. Mater. Chem. A*, 2019, 7, 3344.
- S7 G. Nagaraju, S. M. Cha, S. C. Sekhar and J. S. Yu, *Adv. Energy Mater.*, 2017, 7, 1601362.
- S8 J. Shi, J. Hu, Y. Luo, X. Sun and A. M. Asiri, *Catal. Sci. Technol.*, 2015, 5, 4954.
- S9 R. Xu, R. Wu, Y. Shi, J. Zhang and B. Zhang, *Nano Energy*, 2016, 24, 103.
- S10 C.-Y. Fan, X.-H. Zhang, Y.-H. Shi, H.-Y. Xu, J.-P. Zhang and X.-L. Wu, *Nanoscale*, 2018, 10, 18942.
- S11 Z. Zhuang, Q. Peng, J. Zhuang, X. Wang and Y. Li, *Chem. Eur. J.*, 2006, 12, 211.
- S12 M. Ma, W. Zhu, D. Zhao, Y. Ma, N. Hu, Y. Suo and J. Wang, *Sensor Actuat. B-Chem.*, 2019, 278, 110.
- S13 N. M. Huang, S. Radiman, H. N. Lim, S. K. Yeong, P. S. Khiew, W. S. Chiu, G. H. M. Saeed and K. Nadarajah, *Chem. Eng. J.*, 2009, 147, 399.
- S14 B. Yuan, W. Luan and S.-T. Tu, *CrystEngComm*, 2012, 14, 2145.
- S15 Z.-H. Han, S.-H. Yu, Y.-P. Li, H.-Q. Zhao, F.-Q. Li, Y. Xie and Y.-T. Qian, *Chem. Mater.*, 1999, 11, 2302.
- S16 X. Zhong, L. Zhang, J. Tang, J. Chai, J. Xu, L. Cao, M. Yang, M. Yang, W. Kong, S. Wang, H. Cheng, Z. Lu, C. Cheng, B. Xu and H. Pan, *J. Mater. Chem. A*, 2017, 5, 17954.
- S17 X. Shi, H. Wang, S. Ji, V. Linkov, F. Liu and R. Wang, *Chem. Eng. J.*, 2019, 364, 320.
- S18 Xiong, G. Waller, D. Ding, D. Chen, B. Rainwater, B. Zhao, Z. Wang and M. Liu, *Nano Energy*, 2015, 16, 71.
- S19 H. Peng, J. Zhou, K. Sun, G. Ma, Z. Zhang, E. Feng and Z. Lei, *ACS Sustainable Chem. Eng.*, 2017, 5, 5951.

- S20 G.-F. Chen, Y.-Z. Su, P.-Y. Kuang, Z.-Q. Liu, D.-Y. Chen, X. Wu, N. Li and S.-Z. Qiao, *Chem. Eur. J.*, 2015, 21, 4614.
- S21 C. Wei, Y. Huang, S. Xue, X. Zhang, X. Chen, J. Yan and W. Yao, *Chem. Eng. J.*, 2017, 317, 873.
- S22 Q. Chen, S. Lei, P. Deng, X. Ou, L. Chen, W. Wang, Y. Xiao and B. Cheng, *J. Mater. Chem. A*, 2017, 5, 19323.
- S23 Y. Jiang, Z. Li, B. Li, J. Zhang and C. Niu, *J. Power Sources*, 2016, 320, 13.